Corrosion Science 51 (2009) 518–524

Contents lists available at ScienceDirect

Corrosion Science

journal homepage: www.elsevier.com/locate/corsci

Behaviour of the alloy AA2017 in aqueous solutions of NaCl. Part I: Corrosion mechanisms

M. Bethencourt *, F.J. Botana, M.J. Cano, M. Marcos, J.M. Sánchez-Amaya, L. González-Rovira

Departamento de Ciencia de los Materiales e Ingeniería Metalúrgica y Química Inorgánica, Facultad de Ciencias del Mar y Ambientales, Universidad de Cádiz, Polígono Río San Pedro s/n, Puerto Real-11510, Cádiz, Spain

ARTICLE INFO

Article history:
Received 19 June 2008
Accepted 23 December 2008
Available online 17 January 2009

Keywords:
A. Aluminium
A. Intermetallics
B. EIS
B. SEM
C. De-alloying

ABSTRACT

This paper reports a study carried out on the morphological characteristics the Al–Cu alloy AA2017-T3; its behaviour against corrosion in aqueous solutions of NaCl 0.59 M has been evaluated by immersion during 0–48 h. The techniques employed for this study are SEM and EDS. The results obtained have been verified by electrochemical assays based on monitoring the corrosion potential of the system in OCP, LP and EIS. The behaviour of the intermetallics present in the matrix of the alloy suggests that the design of an effective system of protection should involve the use of cathodic inhibitors.

1. Introduction

The Al–Cu alloys offer excellent ratios of weight to mechanical properties and, for that reason, are commonly employed in the aeronautical industry for numerous structural components. However, they present problems of localised corrosion, especially in media that contain chlorides, due principally to the heterogeneous microstructure of the alloy. This behaviour against corrosion in the aggressive medium must be analysed and characterised for the subsequent design of appropriate systems of protection.

In this context, several authors have made studies of the behaviour of Al–Cu 2xxx alloys against corrosion in media containing chlorides. What has been analysed, basically, is the influence of the intermetallics present in the alloy, using various electrochemical techniques with spatial resolution as SEM (Scanning Electron Microscopy) [1,2], XPS (X-ray Photo Electron Spectroscopy) [2,3], STM (Scanning Tunnelling Microscopy) [4], SKPFM (Scanning Kelvin Probe Force Microscopy) [2,5–9], AFM (Atomic Force Microscopy) [8,10] SIMS (Secondary Ion Mass Spectroscopy) [2,8] y SMRE (Scanning Microreference Electrode) [11].

The results of these studies, based on the alloy AA2024, show that there are two main types of intermetallic particles present: those that are more or less spherical, containing Al(Cu,Mg), and those that are irregular in shape, present in the alloy in the form of clumps or clusters, containing Al(Cu,Fe,Mn). Of these two main types of intermetallic, it is those of Al(Cu,Mg) that are directly related to the corrosion behaviour of the alloy in solutions of NaCl. These intermetallics initially present an anodic character but, by selective desalting, they acquire cathodic properties with respect to the matrix. Thus, after the immersion in NaCl, localised alkaline corrosion (LAC) takes place, due to the cathodic reaction that takes place over these intermetallics; this gives rise to the local increase of the pH, the effect of which is that the aluminium surrounding these intermetallics dissolves. However, the intermetallics of the Al(Cu,Fe,Mn) type remain unaltered, because their electrochemical behaviour is similar to that of the matrix [12].

In this work the behaviour of an Al–Cu alloy, AA2017-T3, in the presence of chlorides, has been studied; this is a high strength alloy with exceptional machining properties [13]. Knowledge of the behaviour of the alloy in NaCl should enable the subsequent design of an appropriate system of protection.

2. Materials and experimental procedure

Samples of the Al–Cu alloy AA2017-T3 measuring $30 \times 25 \times 4$ mm were employed in this study. The composition of this alloy, in percentage by mass, is shown in Table 1.

Before being treated, the samples were polished on SiC paper to a finish of 500 grits. Next the samples were degreased with ethanol and cleaned carefully with distilled water.

For the immersion treatments, aerated aqueous solutions at room temperature of NaCl 0.59 M were employed.

The surface appearance of the samples was studied by Scanning Electron Microscopy (SEM) using an FEG field emission microscope (Sirion model, from Phillips). The microanalysis was performed by

* Corresponding author. Tel./fax: +34 956016154.
E-mail address: manuel.bethencourt@uca.es (M. Bethencourt).

0010-938X/$ - see front matter © 2009 Elsevier Ltd. All rights reserved.
doi:10.1016/j.corsci.2008.12.027

Table 1
Nominal composition of alloy AA2017 (% by mass).

Mg	Mn	Si	Fe	Zn	Ti	Cu	Cr	Al
0.53	0.59	0.62	0.51	0.096	0.03	3.83	0.12	Rest

Energy Dispersive Spectroscopy (XEDS) using an EDAX Spectrometer, Phoenix model, connected to the cited microscope.

The corrosion behaviour was evaluated by continuous current electrochemical techniques: Open Circuit Potential (OCP), Linear Polarisations (LP), and Polarisation Resistance (R_p). But the information that we obtain using these techniques is averaged. For the discriminated evaluation of the protective layer by means of continuous current, in [14] the use is proposed of the parameter Passive Layer Resistance (R_{cp}), which corresponds to the slope on a linear scale of the passive section of the anodic branch of the LP. Although this is also an average term, it gives us information on the resistance of the layer to polarisation. In addition, for the discriminated evaluation of the different subprocesses that contribute to the overall process of corrosion, use can be made of alternating current techniques, such as Electrochemical Impedance Spectroscopy (EIS) [15].

These measurements were conducted in a K235 flat cell, from Parc EG&G, making use of a Solartron model 1287 potentiostat coupled to a Frequency Response Analyser (FRA), model SI 1255 from Solartron. The exposed surface of the working electrode was 1 cm^2. The zone of the impedance spectrum studied corresponds to that in which the responses associated with the intermetallic precipitates and the passive film can be identified. It has been established that this range lies between 10 kHz and 0.01 Hz. The amplitude selected was 5 mV. An Ag/AgCl electrode from Crison (0.207 V/SHE) was utilised as the reference.

3. Results and discussion

The results of the study by SEM and EDS of the microstructure of the alloy AA2017-T3 (Fig. 1) have revealed the presence of different types of intermetallic particles whose composition is comparable with that described by several other authors for alloys of the same group [3,9,16–21]. Firstly, spherical particles with a diameter of 3–5 μm have been identified, with a composition of Al(Cu,Mg), in agreement with [9,16–18]. A second group of particles, of irregular appearance, whose dimensions range from a few micrometers up to 15 μm, are composed of Al(Cu,Fe,Mn); these are present on the surface as both isolated particles and clusters or clumps of several particles [9,17,18]. Other intermetallics of Al(Mg,Si) and (Al,Cu) have also been observed, although these are relatively scarce in the alloy.

In the studies reported in [9,16–18], the atomic percentages of each of the elements that comprise each intermetallic have been determined. Thus, the first type of intermetallic has been assigned a stoichiometry of Al_2CuMg, but the assignment of the second type is more difficult. According to [17], they correspond to (Cu,Mn,-Fe)Al_6 and/or Cu_2FeAl_2.

To make an initial identification of the mechanisms responsible for the corrosion of alloy AA2017 in solution of NaCl, the techniques of SEM and EDS have been employed. SEM images of a sample of alloy AA2017 before and after immersion for 48 h in a solution of NaCl 0.59 M can be observed in Fig. 2. As can be appreciated in this figure, the Al(Cu,Mg) intermetallics are the particles that present more indication of attack. According to [1,11,17,21–23], the Cu in the intermetallics of Al(Cu,Mg) is the principal component responsible for the low resistance of the alloy to particular types of localised corrosion.

From the SEM images in Fig. 3 the change produced in the Al(-Cu,Mg) intermetallics of AA2017, after 48 h of exposure to the

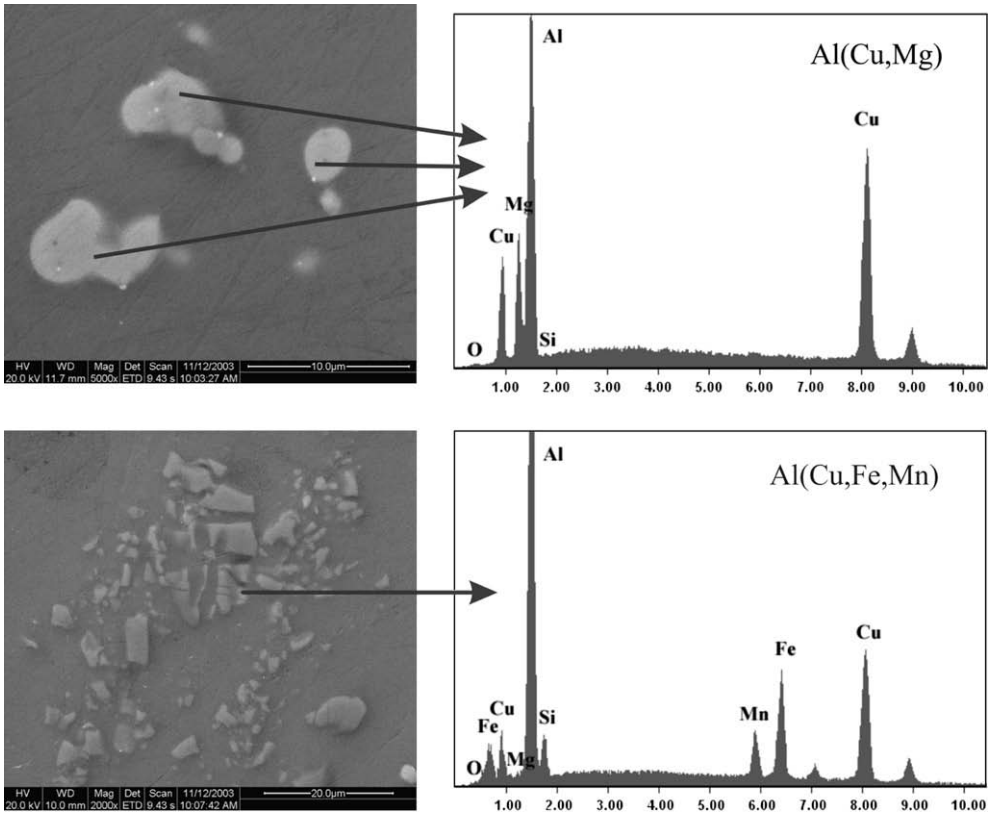

Fig. 1. SEM and EDS images of the principal intermetallic compounds identified in alloy AA2017.

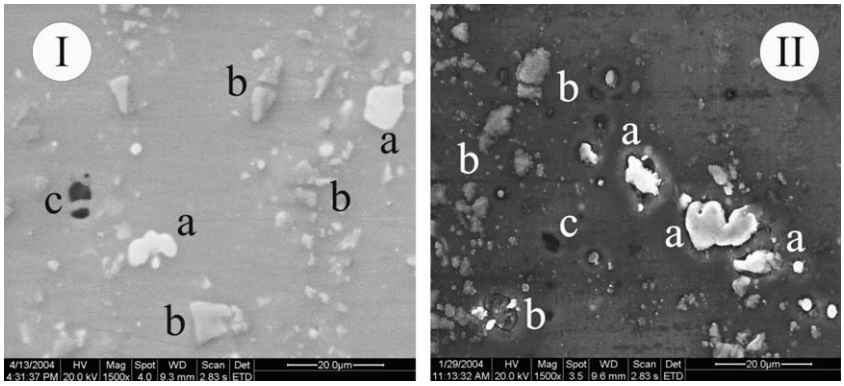

Fig. 2. SEM images for AA2017 (I) before treatment and (II) after immersion for 48 h in NaCl 0.59 M. The intermetallics marked "a" correspond to particles of Al(Cu,Mg); those marked "b" to particles of Al(Cu,Fe,Mn); and those marked "c", to particles of Al(Si,Mg).

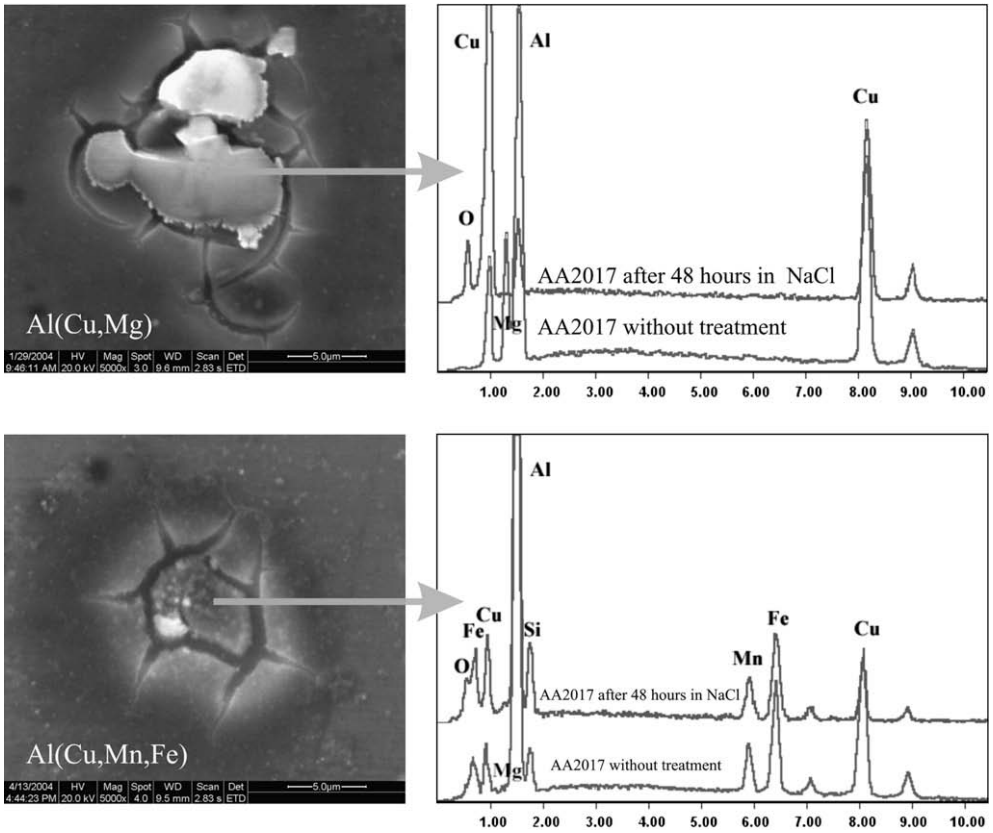

Fig. 3. SEM images and EDS spectra corresponding to the intermetallics of Al(Cu,Mg) and Al(Cu,Mn,Fe) from a sample of AA2017, before and after immersion for 48 h in a solution NaCl 0.59 M.

aggressive medium, can be seen. In the EDS included in this figure, a considerable decrease in the peak of Mg and an increase of the concentration of Cu can be appreciated; these, together with the presence of oxygen, seem to indicate an anodic behaviour of the intermetallic. The resulting anodic process is the selective desalting of Mg which, by the local increase of pH, should precipitate out in the form of an oxide. However, this oxide is not formed. This is because, in the presence of the chloride ions (Cl^-), the $Mg(OH)_2$ is destabilised [24]. The loss of Mg has the effect of enriching the intermetallic in Cu, which subsequently causes the cathodic behaviour of the intermetallics, facilitating the emergence of localised alkaline corrosion, with morphology similar to that described for the alloy AA5083 [25].

This behaviour was also observed for the alloy AA2024 by Shao [11] and Zhu and van Ooij [20]. Thus, although these authors observed that the Al(Cu,Mg) intermetallics were more active than the surrounding matrix, it was confirmed that these were the particles that were acting as cathodes when the samples were exposed to NaCl [9]. This was explained by the phenomenon of selective desalting. When the sample of AA2024 is exposed to NaCl, the intermetallic starts to be more active than the matrix, giving rise to the loss of Mg in a process of selective corrosion. As result, the intermetallic becomes enriched in Cu, which is the cause of the subsequent cathodic behaviour.

Therefore, in first moments of the period of immersion, the anodic process that takes place on these Al(Cu,Mg) intermetallics is the

actual phenomenon of selective desalting of Mg and Al, as a result of the subsequent anodic reactions:

$$Mg \rightarrow Mg^{2+} + 2e^- \quad (1)$$

$$Al \rightarrow Al^{3+} + 3e^- \quad (2)$$

The associated cathodic response is that of reduction of O_2 and/or H_2O, as indicated in reactions (3) and (4), and takes place in the areas of matrix peripheral to the intermetallic:

$$2H_2O + 2e^- \rightarrow H_2 \uparrow + 2OH^- \quad (3)$$

$$O_2 + 2H_2O + 2e^- \rightarrow 4OH^- \quad (4)$$

However, since the intermetallic is being continually desalted, a moment is reached when the intermetallic's behaviour switches from anodic to cathodic, and the cathodic process (3) and (4) then takes place on it. As a result of these reactions, the local pH become more alkaline; hence the layer of aluminium oxide and the aluminium matrix are dissolved according to the reaction:

$$Al_2O_3 + 2OH^-(\text{adsorbed}) \rightarrow 2AlO_2^-(\text{aqueous}) + H_2O \quad (5)$$

In parallel, the oxidation of the metal matrix by uniform corrosion is also taking place, and a layer of aluminium oxide is formed, with the physical detachment of gaseous hydrogen, according to reaction (6):

$$2Al(\text{metal}) + 3H_2O \leftrightarrow Al_2O_3 + H_2 \uparrow \quad (6)$$

While the process of oxidation is taking place, the intermetallic becomes more enriched in copper, and its character is transformed from anodic to cathodic. Thus, the cathodic process of reduction takes place over the intermetallic, and the associated anodic response of the oxidation of aluminium takes place over the neighbouring matrix.

Regarding the other majority types of intermetallic in the alloy, those of Al(Cu,Fe,Mn), these are cathodic in character with respect to the matrix. After 2 h of exposure to the solution of NaCl, these intermetallics remain intact. This suggests that the corrosive attack around these precipitates is less severe than that on those of Al(-Cu,Mg), since the Al(Cu,Fe,Mn) intermetallics are less effective as cathodes. However, after 24 h had elapsed, the samples were then presenting signs of localised attack. This behaviour is similar to that described for alloy AA2024-T4 [12]. Fig. 3 shows the appearance of these intermetallics after the immersion of samples of AA2017 in a solution of NaCl for 48 h.

The absence of oxygen in the EDS and the fact that their composition hardly varies, together with the type of corrosion displayed in the neighbouring aluminium matrix (LAC), tend to confirm the cathodic character of these intermetallics. Thus the process of reduction of O_2 to OH^- takes place on these intermetallics, and the oxidation of the matrix is the associated anodic response. The local increase of the pH is the factor responsible for the dissolution of the layer and matrix in proximity to these intermetallics.

Another notable fact in the behaviour of these intermetallics is the effect of the copper. Thus small superficial particles rich in copper can be seen deposited on the matrix, particularly over the Al(-Cu,Fe,Mn) intermetallics. This has also been observed by other authors for other Al–Cu alloys [16,18,20]. According to these authors, the copper originates from the Al(Cu,Mg) intermetallics themselves; once the Al and Mg in these particles have been desalted, the remaining Cu gets dissolved due to its porous structure. It is this copper in solution that is then reduced on the points of cathodic character, such as the Al(Cu,Fe,Mn) intermetallics, and appears in the form of small nodules.

Thus, in Fig. 4, these small nodules can be seen deposited preferentially on the Al(Cu,Fe,Mn) intermetallic, while no deposition can be seen on the particle of Al(Cu,Mg). We were also able to confirm that the layer of oxide formed around the Al(Cu,Mg) intermetallics is also rich in copper, whereas the layer present around the Al(Cu,Fe,Mn) intermetallics is less rich, Fig. 5.

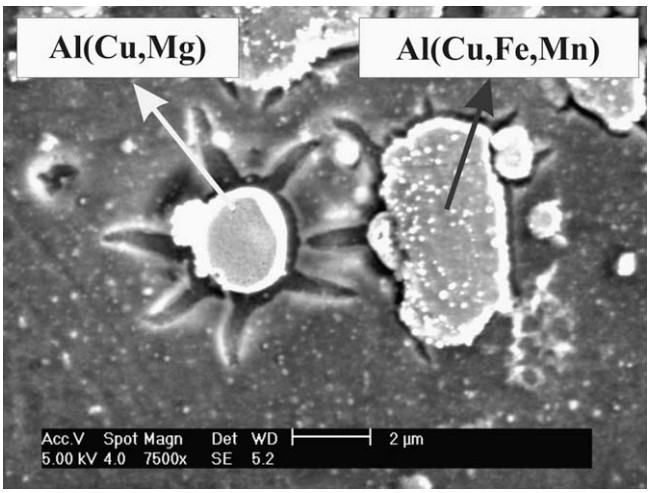

Fig. 4. SEM image of intermetallics of Al(Cu,Mg) and Al(Cu,Fe,Mn) corresponding to alloy AA2017, after immersion for 24 h in a solution of NaCl 0.59 M.

The changes in the composition of the matrix around the intermetallics have been analysed using EDS, taking different points according to their distance from the particular intermetallic examined. Thus, the points analysed include one free from the influence of intermetallics, zones in the proximity of the intermetallic, and zones in which LAC is displayed. With respect to this last zone presenting LAC, its composition in % by mass is very similar to that of the matrix prior to the treatment by immersion in NaCl; this finding is in agreement with what has previously been commented.

Presented in Fig. 5 are the percentage values by mass obtained from the quantification of the EDS of the matrix recorded in function of proximity to intermetallics of Al(Cu,Mg) and Al(Cu,Fe). From the analysis of these results, it can be appreciated that the matrix close to the cathodic intermetallics of Al(Cu,Fe,Mn) contains considerable proportions of oxygen. It is in this zone that the anodic response takes place.

With reference to the matrix in the proximity of the Al(Cu,Mg) intermetallics, the growth of the neighbouring layer can be appreciated, which is indicative of the cathodic character of the intermetallic particle. An increase in the concentration of copper from 7% to 11%, which could originate from the intermetallic itself, has also been detected. In other words, once this type of intermetallic has

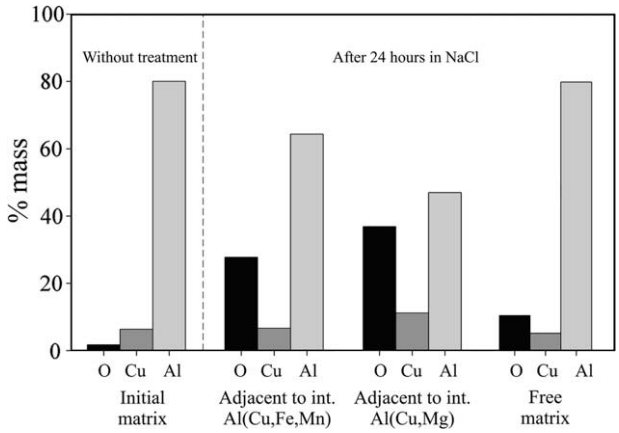

Fig. 5. Variation of the composition of O, Cu and Al, in % of different points of the matrix in function of their proximity to the intermetallics of Al(Cu,Fe,Mn) and Al(Cu,Mg,), before and after exposure to a solution of NaCl 0.59 M for 24 h.

been sufficiently desalted, its porous structure causes the dissolution of the copper; this copper could be precipitated again as an oxide because of the local pH [26] or it could be reduced on cathodic points of the alloy such as the Al(Cu,Mn,Fe) intermetallics [16,18,20].

With the object of verifying what had been observed by means of SEM/EDS, and to obtain the electrochemical parameters related to the corrosion processes (which will be employed in future work as a reference for evaluating the protection provided by systems designed using cerium salts), a series of electrochemical assays was performed. Fig. 6 illustrates the evolution of the open circuit potential of a sample of this Al–Cu alloy in an aerated solution of NaCl 0.59 M. It can be seen in this figure how, in the initial hours, the potential of the sample is about −0.550 V *vs.* Ag/AgCl (0.207 V/SHE) and this value is maintained, until several hours have elapsed when the potential reach to −0.750 V *vs.* Ag/AgCl (0.207 V/SHE).

In this type of system, the initial value of the corrosion potential is determined, partly, by the ohmic drop caused by the natural film of oxide formed during the handling of the sample [27,28]; and its value is partly conditioned by that of the strength of the cathodic process, which depends on the nature of the oxidising agent and on the cathodic area present on the alloy.

In alloy AA2017, aluminium is alloyed principally with copper, which not only is present as part of the intermetallics present (Al(-Cu,Mg)) but is also present, in smaller proportion, in solid solution. This alloying metal alters the potential in the cathodic direction, which explains the initial corrosion potential when a sample of this alloy is exposed to a solution of NaCl. However, as has been seen by SEM/EDS, the intermetallics rich in copper, Al(Cu,Mg), change their behaviour to cathodic in line with the degree of desalting taking place, and even dissolve due to their porous structure. This change of anodic and cathodic areas, together with the decrease of copper on the surface, can lead to the corrosion potential becoming more active as the time of exposure increases. However the potential does not reach a stable value; rather, over the period of time of the assay, it continued to oscillate between the values of −0.600 and −0.700 V *vs.* Ag/AgCl (0.207 V/SHE). This may be due to the fact that not all the intermetallics of Al(Cu,Mg) display the same activity. Therefore, when some of the particles begin to be desalted, the potential of the system is affected. Other authors, such as [29,30] have also reported, for alloy AA2024, variations of the potential towards more active values during OCP assays; this observation has been associated with variations of the ratio of cathodic to anodic areas.

Fig. 7 presents polarisation curves for samples of AA2017 in solution of NaCl, recorded at various times of exposure to the aggressive medium. For the curve obtained at the start of the assay,

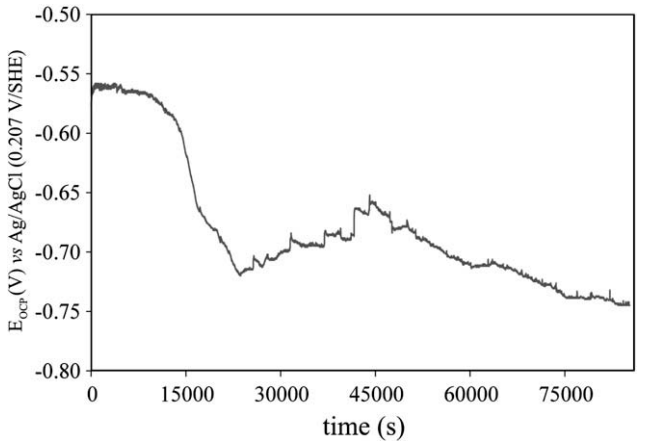

Fig. 6. Evolution with time of the corrosion potential recorded in NaCl 0.59 M during 24 h, for a sample of alloy AA2017.

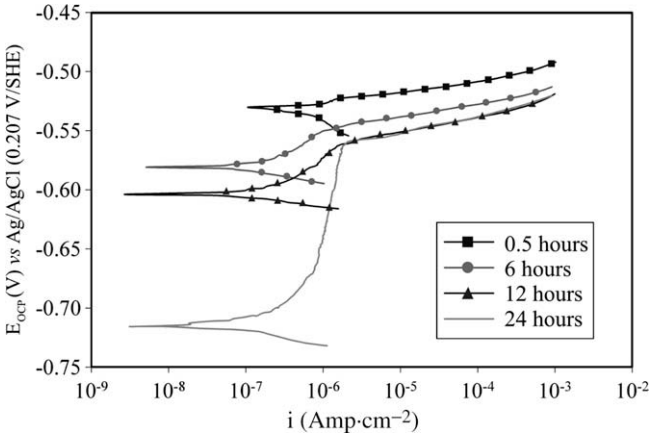

Fig. 7. LP curves for samples of alloy AA2017 immersed in a solution of NaCl 0.59 M, for the periods of time indicated.

it can be observed that the corrosion potential is situated at −0.555 V *vs.* Ag/AgCl (0.207 V/SHE). For potentials slightly higher than the corrosion potential, the density of current is situated at around 10^{-6} A cm^{-2} in a range of potential of some 15 mV. On passing to the anodic branch of −0.540 V *vs.* Ag/AgCl (0.207 V/SHE), the density of current increases sharply due to the intense anodic activity taking place in the system.

On the other hand, a decrease can be observed of the corrosion potential towards increasingly more active values, in the direction of what was seen by means of OCP, while the value of the pitting nucleation potential is maintained at around −0.540 V *vs.* Ag/AgCl (0.207 V/SHE). In any case, although the corrosion potential at initial times is very close to that of pitting nucleation, crystallographic pitting was not seen by SEM, at the exposure times evaluated. The electrochemical parameters given in Table 2 are obtained from evaluation of the linear polarisation shown in Fig. 7.

The value of resistance of the layer, R_{cp}^0, obtained will be employed in a subsequent study to evaluate the tendency to passivity of the protective layers formed in the presence of cerium, from the parameter ΔR_{cp} as a measure of the increase of the resistance of the layer with respect to the value R_{cp}^0 obtained for untreated samples.

$$\Delta R_{cp} = \frac{R_{cp}}{R_{cp}^0} \tag{7}$$

With the object of evaluating, in a discriminated way, the various subprocesses taking place during the corrosion of alloy AA2017 in a solution of NaCl, an analysis by EIS was conducted of the electrochemical response of this system. It was expected that this analysis would turn out to be in good agreement with the observations made by SEM and EDS, and with the results obtained in the study using stationary-state electrochemical techniques.

Represented in Fig. 8 are the EIS diagrams acquired on a sample of alloy AA2017 in the first 24 h of exposure to the solution of NaCl. As can be seen, during the initial moments of the immersion, a first arc is defined in the Nyquist diagram, in Fig. 8(a), which can be assumed to be a superposition of the cathodic activity of the intermetallics and the response of the incipient layer on the matrix, and an inductive loop at low frequencies, which may be associated with

Table 2
Electrochemical parameters obtained from the LP curves of Fig. 7. Surface of the working electrode: 1 cm^2.

E_{OCP} (V) *vs.* Ag/AgCl (0.207 V/SHE)	R_p (kΩ)	R_{cp} (kΩ)
−0.555	5.26	0.93

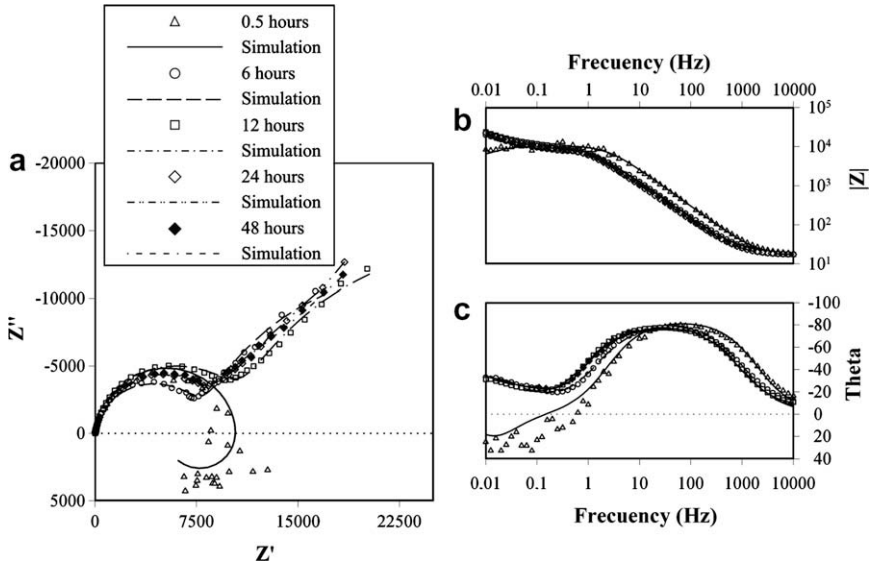

Fig. 8. Impedance spectra for samples of alloy AA2017 immersed in a solution of NaCl 0.59 M for the periods of time indicated. (a) Nyquist diagram; (b) Bode diagram for $|Z|$ and (c) Bode diagram for the phase. Surface of the working electrode: 1 cm^2.

the anodic process presented by the Al(Mg,Cu) intermetallics during the initial stages of exposure to the aggressive medium. According to [31], the presence of an inductive loop may be related to pitting processes. As is well known, pits are formed in aluminium alloys following the crystallographic planes of the matrix [32]. But, as already commented, this type of attack was not observed in the alloy AA2017.

Continuing with the same figure, it can be observed how the inductive loop disappears with time of immersion, and is transformed into a second arc more directly related to the transfer of charge across the interface. The disappearance of the inductive loop is in good agreement with the previous observations, according to which, after the first hours of immersion, the anodic activity of these intermetallics ceases.

For the evaluation of the EIS response of the alloy in solution of NaCl, circuits like those presented in Fig. 9 can be employed. Both

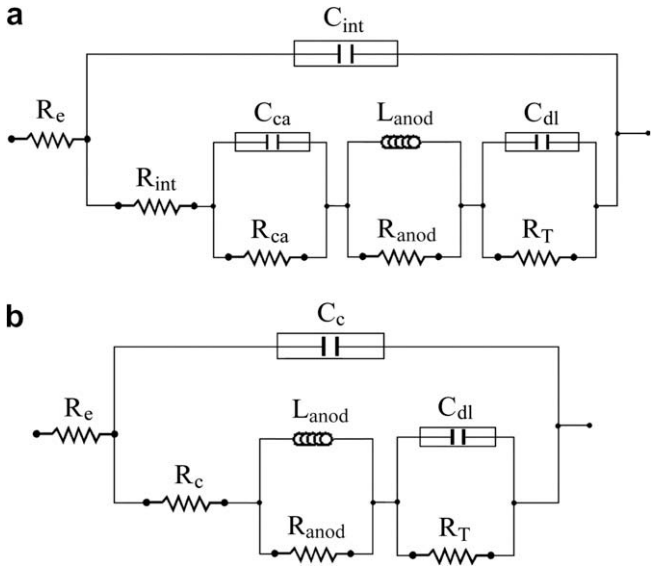

Fig. 9. (a) Equivalent circuit for reproducing the electrical response of alloy AA2017 in a solution of NaCl 0.59 M. (b) Equivalent circuit of the system based on the model of Van der Weijde.

circuits include a R_{anod}–L_{anod} loop that represents the anodic activity on the precipitates of Al(Cu,Mg). For their part, the loops R_{int}–C_{int}, R_c–C_c, R_{ca}–C_{ca} and R_T–C_{dl} have a meaning similar to that described recently for other aluminium alloys [33]. R_{int}–C_{int} is the loop associated with the reactions that take place around the intermetallics; the loop R_{ca}–C_{ca} represents the response of the layer; R_T is the charge transfer resistance; and C_{dl} is the capacity of the double layer. This last loop gives information on the slower processes that take place in the system. In addition, the loop R_{anod}–L_{anod} disappears after a few hours of immersion, and so it is only employed to reinforce the observations previously made.

Table 3 gives the values of each of the parameters related to the layer, obtained from the fit of the impedance spectra recorded for the circuits proposed. What is notable in this table is the response in impedance of the intermetallics of cathodic character, which begin to present LAC attack after several hours of immersion in NaCl have elapsed. Although the R_{int} remains more or less constant over the time of study, the capacity term C_{int} continues increasing, with the increase being greater after 6 h of immersion. This may be explained considering the expression for the capacity proposed in [34]:

$$C = \varepsilon_0 \varepsilon \frac{s}{d} \tag{8}$$

Thus, at the moment when the Al(Cu,Mg) intermetallics switch to behaving as cathodic points, there is a considerable increase in the area relative to these intermetallics and, therefore, there is an increase in the term C_{int}.

On the other hand, referring to the layer formed on the metal matrix, the term C_{ca} commences increasing with time of exposure. The increase of R_{ca} may indicate that this increase of C_{ca} is due basically to the increase in area of the layer spreading over the matrix. After 6 h, C_{ca} begins to decrease while R_{ca} continues increasing. In accordance with Eq. (8) and the SEM observations, this may be associated with an increase in the thickness of the layer.

4. Conclusions

The results obtained demonstrate that the intermetallics present in alloy AA2017 are responsible for its behaviour in a solution of NaCl 0.59 M. Thus, the Al(Cu,Mg) intermetallics initially present an anodic behaviour with respect to the matrix, giving rise to a pro-

Table 3
Values of the elements related to the layer, determined from the fit to the models of Fig. 9, of the EIS response of alloy AA2017 immersed in a solution of NaCl 0.59 M, at the times indicated. Surface of the working electrode: 1 cm^2.

t (h)	C_c ($\mu F\ cm^{-2}$)	φ_c	R_c ($k\Omega\ cm^2$)	C_{int} ($\mu F\ cm^{-2}$)	φ_{int}	R_{int} ($\Omega\ cm^2$)	C_{ca} ($\mu F\ cm^{-2}$)	φ_{ca}	R_{ca} ($k\Omega\ cm^2$)
0.25	8.79	0.937	4.60	4.20	0.979	11.09	2.95	0.881	4.68
0.5	10.44	0.929	6.10	4.32	0.964	12.77	5.87	0.908	6.19
1	10.34	0.928	9.05	4.26	0.959	14.61	5.63	0.918	8.93
2	11.74	0.871	3.80	4.97	0.968	20.74	6.96	0.912	3.55
4	14.74	0.924	6.83	4.12	0.985	11.01	10.19	0.903	6.80
6	19.79	0.907	11.30	6.14	0.934	6.94	12.65	0.901	11.10
8	19.10	0.908	11.05	7.74	0.914	7.63	11.02	0.911	11.04
10	19.74	0.907	11.98	8.80	0.909	7.99	10.51	0.914	11.72
12	23.30	0.903	10.62	11.71	0.887	7.92	9.27	0.929	11.92
18	23.23	0.903	10.42	15.93	0.883	9.21	7.17	0.943	10.28
20	21.82	0.905	12.08	17.49	0.901	7.50	4.08	0.928	12.20
24	23.70	0.900	10.25	17.64	0.906	5.17	5.86	0.898	10.36
48	24.10	0.890	10.05	17.76	0.908	5.01	5.84	0.886	10.12

cess of selective desalting of Mg and Al. As a result of this, there is an increase in the concentration of Cu in these intermetallics, which is the cause of their subsequent cathodic behaviour. The process of reduction of oxygen to OH^- takes place as the cathodic response. The local increase of the pH causes the dissolution of the layer of oxide and of the neighbouring aluminium.

On the other hand, the Al(Cu,Fe,Mn) intermetallics display a cathodic behaviour with respect to the matrix, and a reaction of reduction of oxygen takes place over these. The associated anodic response is the oxidation of the matrix. Similarly, the local increase of the pH produces the dissolution of the layer of oxide and of the matrix that surrounds these intermetallics.

Having now identified the corrosion processes that take place when the alloy AA2017 is exposed to solutions of NaCl, it is reasonable to believe that an effective system of protection, alternative to the use of Cr(VI), can be designed based on the employment of cathodic inhibitors such as cerium salts.

References

[1] H.M. Obispo, L.E. Murr, M. Arrowood, E.A. Trillo, Copper deposition during the corrosion of aluminum alloy 2024 in sodium chloride solutions, J. Mater. Sci. 35 (14) (2000) 3479–3495.
[2] J.V. Kloet, A.W. Hassel, M. Stratmann, Effect of pretreatment on the intermetallics in aluminum alloy 2024-T3, Z. Phys. Chem. 219 (11) (2005) 1505–1518.
[3] C. Blanc, B. Lavelle, G. Mankowsk, The role of precipitates enriched with copper on the susceptibility to pitting corrosion of the 2024 aluminium alloy, Corros. Sci. 39 (3) (1997) 495–510.
[4] R.C. Bhardwaj, A.G. Martin, J. ÓM Bockris, In situ corrosion studies of aluminum and aluminum tantalum alloy in 0.01 M NaCl using STM, J. Electrochem. Soc. 139 (1992) 1050–1058.
[5] P. Schmutz, G.S. Frankel, Characterization of AA2024-T3 by scanning Kelvin probe force microscopy, J. Electrochem. Soc. 145 (7) (1998) 2285–2295.
[6] P. Schmutz, G.S. Frankel, Corrosion study of AA2024-T3 by scanning Kelvin probe force microscopy and in situ atomic force microscopy scratching, J. Electrochem. Soc. 145 (7) (1998) 2295–2306.
[7] P. Leblanc, G.S. Frankel, A study of corrosion and pitting initiation of AA2024-T3 using atomic force microscopy, J. Electrochem. Soc. 149 (6) (2002) B239–B247.
[8] L. Lacroix, L. Ressier, C. Blanc, G. Mankowski, Combination of AFM, SKPFM, and SIMS to study the corrosion behavior of S-phase particles in AA2024-T351, J. Electrochem. Soc. 155 (4) (2008) C131–C137.
[9] T.J. Warner, M.P. Schmidt, F. Sommer, D. Bellot, Characterization of corrosion initiation on 2024 aluminum alloy by atomic force microscopy, Z. Metallkd. 86 (1995) 494–501.
[10] P. Campestrini, E.P.M. Van Westing, H.W. Van Rooijen, J.H.W. De Wit, Relation between microstructural aspects of AA2024 and its corrosion behaviour investigated using AFM scanning potential technique, Corros. Sci. 42 (11) (2000) 1853–1861.
[11] M. Shao, Y. Fu, R. Hu, C. Lin, A study on pitting corrosion of aluminum alloy 2024-T3 by scanning microreference electrode technique, Mater. Sci. Eng. A 344 (1–2) (2003) 323–327.
[12] J. Aldykewicz, H.S. Isaac, A.J. Davenport, Investigation of cerium as a cathodic inhibitor for aluminum–copper alloys, J. Electrochem. Soc. 142 (1995) 3342–3350.
[13] S.F. Rudy, Aluminum designations information clarification, Plat. Surf. Finis. 94 (10) (2007) 29–32.
[14] A. Aballe, M. Bethencourt, F.J. Botana, M.J. Cano, M. Marcos, On the mixed nature of cerium conversion coatings, Mater. Corros. 53 (2002) 176–184.
[15] R.J. Scully, Electrochemical methods of corrosion testing, in: J.R. Davis, J.D. Destefani (Eds.), Corrosion, Metal Handbook, vol. 13, ninth ed., ASM International, Ohio, 1989, pp. 212–220.
[16] V. Guillaumin, G. Mankowski, Localized corrosion of 2024 T351 aluminium alloy in chloride media, Corros. Sci. 41 (3) (1998) 421–438.
[17] M. Gao, C.R. Feng, R.P. Wei, An analytical electron microscopy study of constituent particles in commercial 7075-T6 and 2024-T3 alloys, Metall. Mater. Trans. A 29 (4) (1998) 1145–1151.
[18] R.G. Buchheit, R.P. Grant, P.F. Halva, B. Mckenzie, G.L. Zender, Local dissolution phenomena associated with S phase (Al_2CuMg) particles in aluminum alloy 2024-T3, J. Electrochem. Soc. 144 (8) (1997) 2621–2628.
[19] G.S. Chen, M. Gao, R.P. Wei, Microconstituent-induced pitting corrosion in aluminum alloy 2024-T3, Corrosion 52 (1) (1996) 8–15.
[20] D. Zhu, W.J. van Ooij, Corrosion protection of AA2024-T3 by bis-[3-(triethoxysilyl)propyl]tetrasulfide in sodium chloride solution. Part 2. Mechanism for corrosion protection, Corros. Sci. 45 (10) (2003) 2163–2197.
[21] T. Suter, R.C. Alkire, Microelectrochemical studies of pit initiation at single inclusions in Al 2024-T3, J. Electrochem. Soc. 148 (1) (2001) B36–B42.
[22] C.M. Liao, R.P. Wei, Galvanic coupling of model alloys to aluminum—a foundation for understanding particle-induced pitting in aluminum alloys, Electrochim. Acta 45 (1) (1999) 881–888.
[23] R.G. Buchheit, Compilation of corrosion potentials reported for intermetallic phases in aluminum alloys, J. Electrochem. Soc. 142 (1995) 3994–3996.
[24] E. Ghali, Magnesium and magnesium alloys, in: R.W. Revie (Ed.), Uhlig's Corrosion Handbook, second ed., John Wiley & Son Inc., New York, 2000, pp. 793–830.
[25] A. Aballe, M. Bethencourt, F.J. Botana, M.J. Cano, M. Marcos, Localized alkaline corrosion of alloy AA5083 in neutral 3.5% NaCl solutions, Corros. Sci. 43 (9) (2001) 1657–1674.
[26] R.C. Weast (Ed.), Handbook of Chemistry and Physics, 55th ed., Section B (The elements and inorganic compounds), CRC Press, Cleveland, Ohio, 1974.
[27] S.M. Moon, S.I. Pyun, Faradaic reactions and their effects on dissolution of the natural oxide film on pure aluminum during cathodic polarization in aqueous solutions, Corrosion 54 (7) (1998) 546–552.
[28] A. Aballe, M. Bethencourt, F.J. Botana, M. Marcos, J. Pérez, M.A. Rodríguez, Green inhibitors. Rare earth based systems, Rev. Metal. Madrid 33 (6) (1997) 363–369.
[29] J.W.J. Silva, A.G. Bustamante, E.N. Codaro, R.Z. Nakazato, L.R.O. Hein, Morphological analysis of pits formed on Al 2024-T3 in chloride aqueous solution, Appl. Surf. Sci. 236 (2004) 356–365.
[30] G.O. Llevbare, Inhibition of pitting corrosion on aluminum alloy 2024-T3: effect of soluble chromate additions vs. chromate conversion coating, Corrosion 56 (3) (2000) 227–242.
[31] A. Aballe, M. Bethencourt, F.J. Botana, M. Marcos, M.A. Rodríguez, Corrosion Monitoring of the AA2024 alloy in NaCl solutions by electrochemical noise measurements, Rev. Metal. Madrid 34 (1998) 42–46.
[32] I.L. Mueller, J.R. Galvele, Pitting potential of high purity binary aluminium alloys. II. Al–Mg and Al–Zn alloys, Corros. Sci. 17 (1977) 995–1007.
[33] M. Bethencourt, F.J. Botana, M.J. Cano, M. Marcos, J.M. Sánchez-Amaya, L. González Rovira, Using EIS to analyse samples of Al–Mg alloy AA5083 treated by thermal activation in cerium salt baths, Corros. Sci. 50 (5) (2008) 1376–1384.
[34] J.B. Bessone, D.R. Salinas, C.E. Mayer, M. Ebert, W.J. Lorenz, An EIS study of aluminium barrier-type oxide films formed in different media, Electrochim. Acta 37 (12) (1992) 2283–2290.